

## Automated compatibility checking of prefabricated components using 3D as-built models and BIM

Mojtaba Noghabaee\*, Yajie Liu, Kevin Han

*Department of Civil, Construction, and Environmental Engineering, North Carolina State University, NC, USA*



### ARTICLE INFO

**Keywords:**  
 Point cloud  
 Reality capture  
 Computer vision  
 Visual data  
 Laser scan

### ABSTRACT

There have been recent efforts to use reality capture technologies to perform remote quality control in construction. However, there is a lack of research efforts in detecting construction incompatibilities in modular construction using reality capture technologies. The construction incompatibilities in modular construction often cause reworks and delays in the project schedule. To address this issue, this paper presents a general compatibility analysis method that propose scanning the modules in manufacturing plant and construction site, and check module-to-module compatibility remotely, prior to the shipment and installation. This study provides three sample module-to-module compatibility scenarios to validate the proposed compatibility analysis. The case study results show that the compatibility analysis method was able to identify the compatibility issues with high accuracy. Lastly, the compatibility analysis method was validated in terms of accuracy and time performance in six scenarios that was defined on the modules.

### 1. Introduction

The architecture, engineering, and construction (AEC) industry is among the largest industries in the U.S., spending over \$1.3 trillion in 2019 [1,2]. In response to rising construction demand and a severe shortage of skilled labor in the workforce [3,4], developers and contractors worldwide are now revisiting the concept of offsite construction, integrating new technologies and manufacturing approaches, such as robotics and reality capture [5,6]. Moving major parts of construction into large manufacturing plants introduced new opportunities, such as global construction, allowing, parts of a module or building components are produced from different countries where labor and material are cheaper and then shipped to the construction site. By employing modular construction the required on-site labor was decreased by 70%, which shows that modular construction can be one way to deal with labor shortage that is affecting the construction industry in the U.S. [3,4]. While speed and cost were the primary drivers behind Marriott's and many other companies' use of offsite construction, this approach provides other benefits. For instance, constructing modules under controlled environments allows quality to be vastly improved because manufacturing is not affected by weather conditions. Unlike construction sites that is constantly changing, there is no change in the environment and the manufacturing facilities covers multiple construction

projects without changing their locations, allowing consistency in quality. Also, prefabrication can significantly reduce waste in the construction process, limiting the overall environmental impact of construction [7,8].

Despite these benefits, offsite manufacturing often introduces significant challenges that need to be addressed. One of the challenges in modular construction is module mismatch, which often causes delays for the whole project [9,10]. Modules often need to be modified on-site to fix the incompatibilities, which increase rework and introduce new challenges. If modules are not repairable on-site, remanufacturing and shipping will lead to even greater delays and cost overruns. To avoid rework and remanufacturing, researchers suggested using laser scanners and BIM for quality assessment [11]. The researchers suggested registering the as-built point clouds of the modules to the BIM and manually or automatically detect geometric defects [11]. Using this approach, geometric defects can be identified at the manufacturing facility before shipment. Researchers have applied this concept to various types of modules, such as piping spools [12], precast concrete modules [13,14], and industrial modules [11].

The main limitation of the current methods in detecting the geometric defects is that the modules are investigated individually. However, the defects often occur in module-to-module incompatibilities, especially when there is a discrepancy or error in the design model

\* Corresponding author.

E-mail address: [m.noghabaee@gmail.com](mailto:m.noghabaee@gmail.com) (M. Noghabaee).

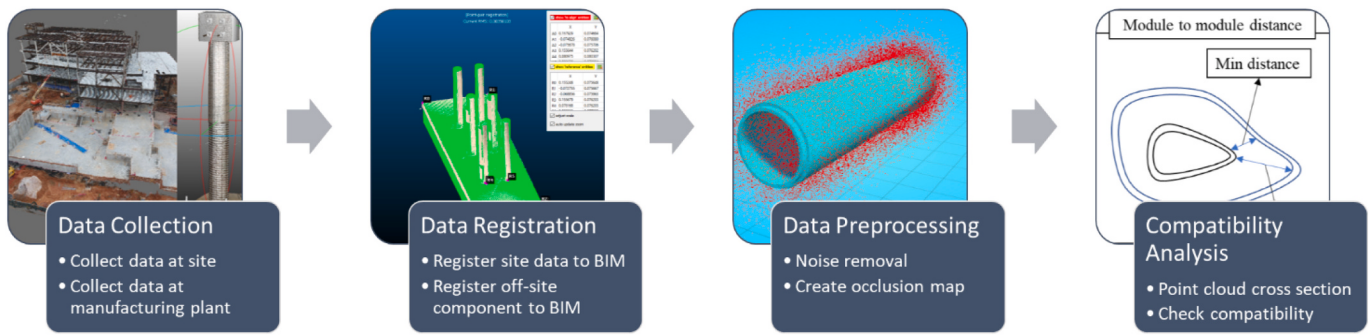


Fig. 1. Method overview and steps.

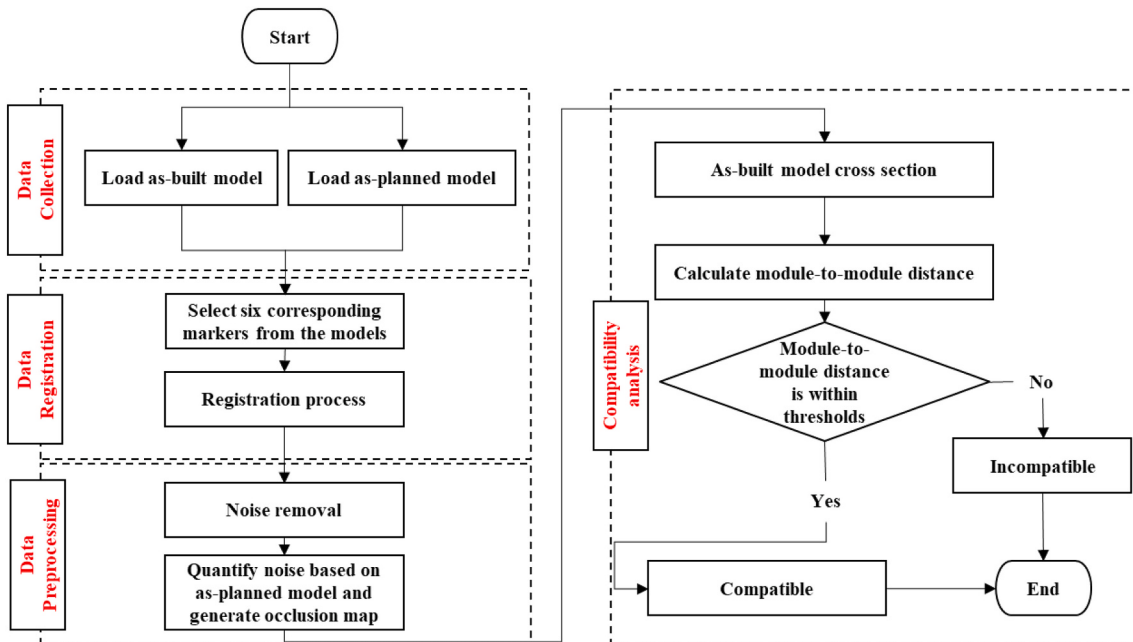


Fig. 2. Flowchart of the compatibility analysis.

versus the as-built. For example, a piping module may not be compatible with its connecting modules due to changing site conditions even if each module meets the required geometric standards. To address this limitation, this paper presents a compatibility checking framework. In this framework, modules in the manufacturing facilities and the main structure on the project site are scanned. The presented semi-automated compatibility assessment method detects module-to-module incompatibilities prior to the shipment from the manufacturing sites to the project site.

Previous research efforts are only focused on the quality assessment of a single module or component based on the corresponding BIM model of the same module or component. Meaning that, even if a module passes quality requirement compared to its design model, there still is a risk of incompatibility with other connecting parts on the jobsite due to constant changing nature of construction [15–17]. The development of compatibility checking system between as-built modules is challenging since checking the compatibility among 3D scanned models with different geometry, meshing, and occlusion is inherently dynamic and can vary widely [18]. Also, BIM and scanned models have a large number of vertices and faces, which may be challenging for near real-time applications. Moreover, researchers suggested a need for generalized quality assessment methods that can be applied on various types of modules [19]. Lastly, researchers identified that the noise and occlusions are two factors that can adversely affect the accuracy of the

proposed quality assessments methods [20]. The presented method in the following section attempts to address these gaps in knowledge.

The main contributions of this study are 1) a compatibility assessment method that checks compatibility between two modules and quantifies the gap between them, ensuring quality of fabricated components before they are shipped and assembled and 2) a generalized method that work with different types and shapes of modular/fabricated components. This compatibility method was tested and validated using three types of offsite manufactured modules with varying shapes.

## 2. Background

Over the past few years, reality capturing technologies have received significant popularity in the AEC industry, namely construction progress and performance monitoring [21–23], assembly training [15], construction quantity takeoff [24], safety [25], and inspection [23,26]. However, there are still numerous research questions to be investigated.

Module misplacement has always been a challenge in construction. Research studies wanted to avoid this by employing new technologies that can automatically detect the misplacement [27]. Researchers proposed using point clouds to detect module position mismatch based on scan-to-BIM registrations in pipe spools [28], however this method works only on uncluttered point clouds [29]. Beside point clouds, researchers suggested using video surveillance to detect the position of

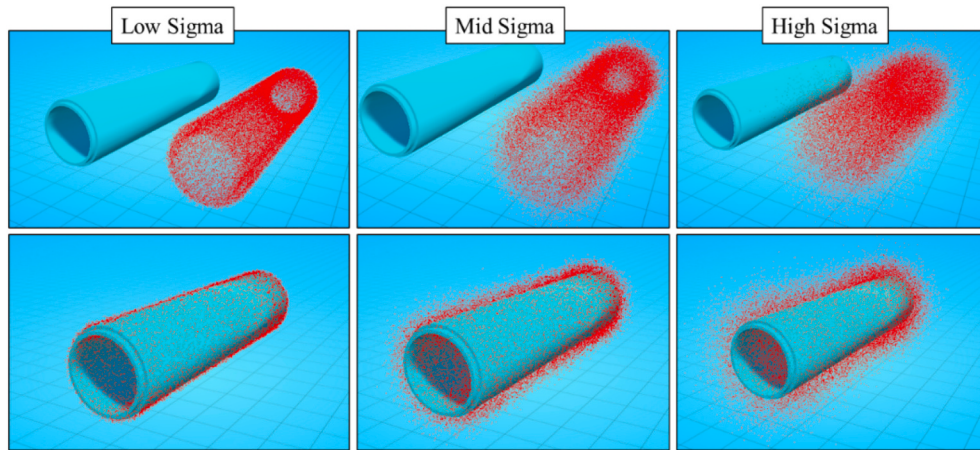


**Fig. 3.** Generated point clouds with different levels of Gaussian noise for a sample pipe.

precast concrete modules [30]. Also, researchers proposed a technique that can accurately estimate rebar positions on reinforced precast concrete bridge deck panels [19]. Researchers presents an algorithm for automated discrepancy quantification of construction components [29,31]. The common limitation of all of these studies was that their system only works for a single module under a certain condition and the proposed method could not be used on wide variety of modules [29,31].

In addition to the modules position, module dimension is another important factor. Researchers proposed automated systems that uses scan-to-BIM registration to perform dimensional quality assessment of precast concrete elements [32,33]. Similar methods performed quality assessments on the concrete steel embedded plates [34]. Researchers expanded the methods to measure rebar sizes [14] and module dimensions [35]. Ultimately, researchers focused on detected module defects such as warping in precast concrete modules [33] and deflection of the bridges for maintenance [36]. They suggested using octree and voxelization to measure the bridge deflections [36]. However, their suggested method is only applicable to the bridge maintenance and could not be used on various construction elements [36]. Also, the researchers developed methods to automatically detect the squareness of shear keys in a precast concrete module [13].

Their main limitation was that their method was only applicable on small size modules. Lastly, researchers suggested geometric quality inspection technique to detect defects for prefabricated MEP modules [11] and a framework for surface quality assessment of precast concrete elements using edge extraction algorithms [32,33].

### 3. Method

**Fig. 1** illustrates the overall steps of the developed compatibility checking method. The laser scanning data from two modules that need to be assembled together is collected using a laser scanner. An example for such modules can be two mechanical, electrical and plumbing (MEP) modules which need to be matched accurately. After data collection, the modules will be registered to the BIM model. This operation is performed semi-automatically by method similar to [37]. After registering each module to the corresponding BIM element, the noise of each point cloud needs to be quantified and removed to make sure the collected point cloud passes the requirement for compatibility checking. Lastly, a compatibility analysis has been done on both modules to make sure the modules pass the compatibility requirements. Also, during the compatibility analysis, the incompatible parts of each module will be highlighted to the user.

**Fig. 2** shows the overall workflow and provide more detail for each step that was mentioned in **Fig. 1**. The red boxes show the compatibility checking method, the main contributions of this paper. The output of

this system is going to show whether the two modules are going to be compatible (i.e., fit, joint, attached as designed) based on the quality threshold selected by the user.

#### 3.1. Data collection

This section describes the process of data collection. As-built modeling needs to be performed at two different places – 1) where a module of interest is manufactured and 2) where this module is shipped to and assembled. To generate the 3D as-built models of the module and its connecting part (i.e., building component), a reliable reality capture technology should be used. For instance, for larger module and building components, a terrestrial laser scanner can be used. For smaller modules and/or models with very stringent quality requirements, a metrology-grade laser scanner should be used. The 3D CAD/BIM models of two objects are also needed.

#### 3.2. Data registration

The registration process can use any existing registration method (i.e., automated [38], semi-automated [39,40], or manual). For this study, a semi-automated registration was performed similar to [39,40]. Six corresponding points (features or markers) were selected from both BIM and the point cloud to register the point cloud to the BIM. Through this registration, the two modules' point clouds are appropriately positioned for a compatibility check. This step is necessary since checking the module-to-module compatibility is not possible without placing the point clouds to their installation location. The corresponding points were used to solve the least square registration problem of absolute orientation for seven degrees of freedom [41], which returns a transformation matrix and a registration error. The transformation matrix is used to perform a 3D linear transformation [42,43]. In case of a high registration error, the registration has to be iterated until the accuracy of the registration reaches below the user requirement/threshold. Also, other methods can be used for registration including automated registration using fiducial markers and surveying coordinates. In this research, we only focus on the module-to-module interaction, and we assume that the elements already passed the dimensional qualities with respect to their BIM models. Several past studies suggested methods to compare BIM and Scan models [15,44].

#### 3.3. Data preprocessing

In addition to registration, noise is also another essential factor that can affect the compatibility checking process. Excessive noise can severely affect compatibility checking. **Fig. 3** shows a sample point cloud

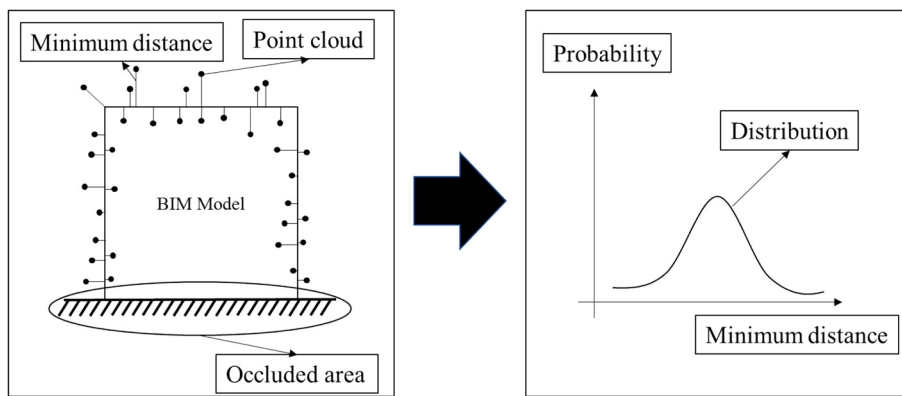


**Fig. 4.** Extraction of noise distribution based on scanned point cloud to BIM registration.

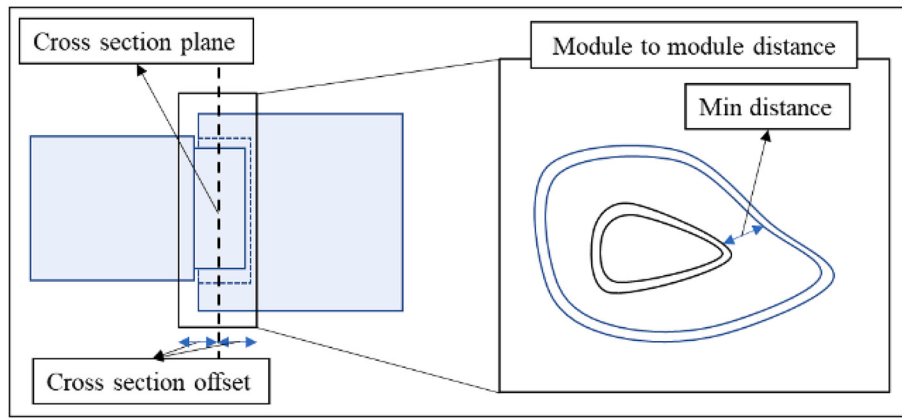


**Fig. 5.** Visualizing the features selected for compatibility analysis.

that was affected by Gaussian noise with different levels of standard deviation. The point clouds in Fig. 3 has been generated synthetically to shows that high standard deviation can adversely affect the compatibility, meaning that the noise cancellation must be applied. The standard deviation should be kept low in accordance with user quality requirement to make compatibility checking feasible.

Fig. 4 illustrates the process to quantify noise based on point cloud-to-BIM registration. After they are registered into the same coordinate system, the minimum distance between each point in the point cloud to the BIM is calculated. These minimum distances form a probability distribution which presents the distribution of noise in the point cloud as illustrated in Fig. 4.

The noise quantification method operates based on the following mathematical definitions, operations, and steps that compare BIM and scan models. A point cloud  $PC_1$  is defined as a number of points that consists of  $(V_1, V_2, \dots, V_n)$ . Each point  $V$  is created from three values for a 3D coordinate (i.e.,  $x, y, z$ ) and  $n$  is the total number of points in point cloud  $PC$ . Similarly, a CAD/BIM model consists of triangulated planar surfaces/meshes that consists of vertices. Each face  $F$  is created by connecting three vertices  $(V_i, V_j, V_k)$ . Therefore, a mesh is defined as  $M(V, F)$ . Noise is defined as the distance between each point ( $V_i$ ) in the point cloud  $PC_1$  and the BIM (mesh  $M$ ). First, noise mean and standard deviation is computed and the point cloud went through a noise removal process. To remove any potential noise in the collected point clouds, the Statistical Outlier Removal (SOR) method [45,46] was applied. After the noise removal process, noise mean and standard deviation was calculated another time to ensure that the noise level is below the selected threshold by the user.

In this study, we only mark the parts that are missing in the scanned model by comparing it to its corresponding BIM model as suggested in

this section. The missing parts in the scanned model could be a result of either occlusion or the missing a part in the module. In either scenario, we are not going to make any decision about the missing section of the module and the algorithm is not going to make any decision based on that section. In addition, please note that the main assumption of this research is that the module is built according to its BIM model and any incompatibility between BIM and scan is detected prior to the compatibility checking process. Several studies discussed methods that are capable of comparing scan to BIM and those methods were discussed in the background section. Also, to ensure that the compatibility analysis is robust to false negatives, the top-grade laser scanners have to be used and the data has been inspected carefully.

### 3.4. Compatibility analysis

Compatibility of the two modules is checked at each cross section (the interval of the cross sections can be determined by the users). Cross section planes are going to be in all directions (i.e.,  $x, y, z$ ) and with selected offset, where a section plane and offset are selected by the users as illustrated in the Fig. 5. In other words, offset is the amount that the point cloud is clipped. The cross section of a point cloud  $PC$  is defined as follows:

$$\text{cross section} = v, \text{where, } \text{section} - \text{offset} < v < \text{section} + \text{offset} \quad (1)$$

where  $v$  is a point in point cloud,  $\text{section}$  is the coordinate of section plane, and  $\text{offset}$  is coordinate of offset planes as illustrated in Fig. 5.

Ultimately, the module-to-module distance was checked for each cross section. If the minimum distance between two modules in each cross section passed the upper and lower thresholds, the modules are



**Fig. 6.** Sample case studies for compatibility analysis.

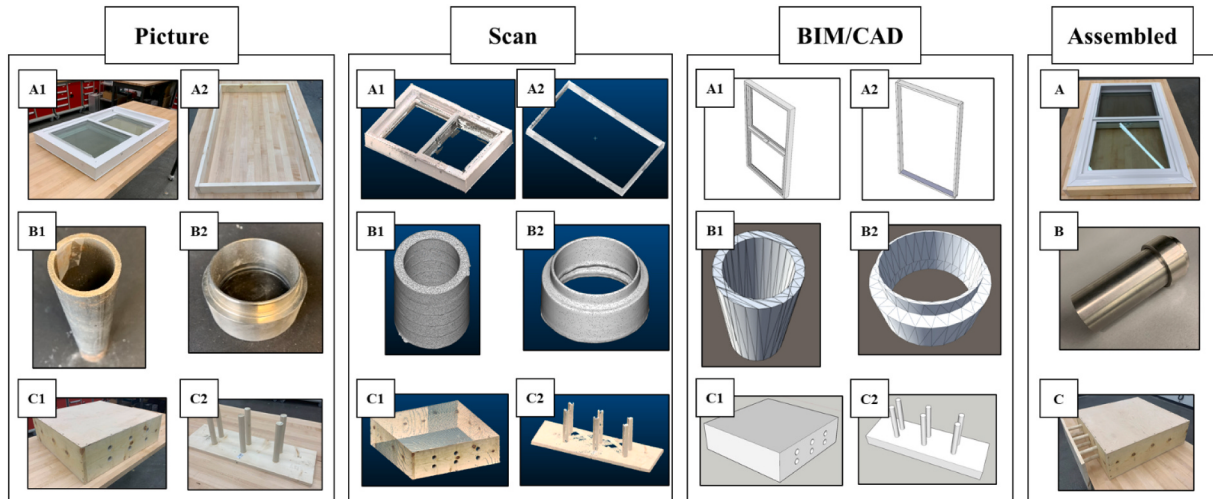


**Fig. 7.** Scan vs. BIM/CAD model of the used objects.



**Fig. 8.** Scanning setup with Faro laser scanner.

**Table 1**

Point count and face count of the point clouds in scan and BIM.

|             |      | Point cloud |        |           |         |         |        |
|-------------|------|-------------|--------|-----------|---------|---------|--------|
|             |      | A1          | A2     | B1        | B2      | C1      | C2     |
| Face count  | BIM  | 2532        | 124    | 384       | 448     | 1176    | 1180   |
| Point count | Scan | 254,156     | 93,835 | 1,000,026 | 999,873 | 193,687 | 48,114 |

**Table 2**

Registration error for each marker set on each model in millimeter.

| Objects | Markers |     |     |     |     |     |
|---------|---------|-----|-----|-----|-----|-----|
|         | M1      | M2  | M3  | M4  | M5  | M6  |
| A1      | 3.1     | 2.3 | 1.1 | 1.8 | 2.6 | 3.4 |
| A2      | 2.2     | 2.9 | 3.9 | 3.4 | 1.6 | 1.2 |
| B1      | 1.8     | 3.2 | 5.3 | 3.2 | 1.3 | 1.7 |
| B2      | 2.6     | 1.3 | 1.6 | 4.1 | 1.0 | 0.6 |
| C1      | 1.6     | 2.7 | 4.0 | 2.5 | 0.8 | 4.9 |
| C2      | 1.4     | 2.3 | 4.9 | 1.8 | 5.6 | 2.5 |

**Table 3**

Model error specifications after artifact removal (before noise removal).

|           | Objects |         |         |         |         |         |
|-----------|---------|---------|---------|---------|---------|---------|
|           | A1      | A2      | B1      | B2      | C1      | C2      |
| Mean (mm) | 12 (58) | 18 (76) | 8 (16)  | 6 (22)  | 15 (34) | 14 (31) |
| Sigma     | 31 (46) | 27 (32) | 22 (37) | 17 (29) | 17 (44) | 11 (57) |

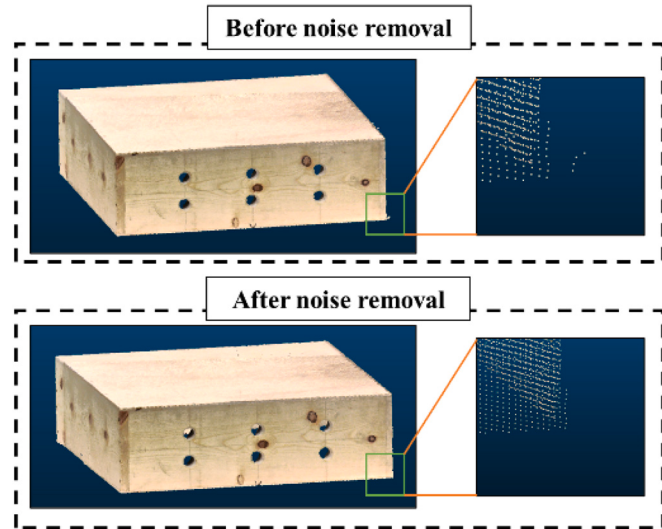


Fig. 9. Sample demonstration of noise removal on object C1 in Fig. 7.

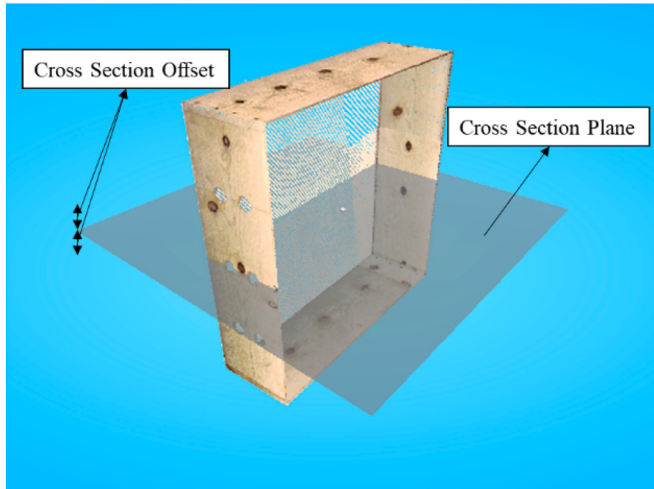


Fig. 10. Point cloud cross section for C1.

compatible. Otherwise, the modules are marked as incompatible. The upper bound threshold is the maximum tolerable gap, and the minimum threshold is the minimum tolerable gap. The lower value for the thresholds corresponds to tighter joint where higher values of the thresholds correspond to having more gap between the elements. The proposed compatibility assessment uses the minimum distance ( $MD$ ) between two modules. The module-to-module minimum distance ( $MD$ ) between the two point clouds,  $PC_1$  and  $PC_2$ , is defined as follows:

$$MD = \min \left( \left| V_i^1 - V_j^2 \right| : i \in \{1 : n_1\} \right) \quad (2)$$

where  $V_i^1$  is a point in point cloud  $PC_1$  and  $V_j^2$  is a point in point cloud  $PC_2$ . Also,  $n_1$  and  $n_2$  are the number of points in  $PC_1$  and  $PC_2$  respectively.

#### 4. Experimental setup and results

This section summarizes the experimental setup and results. To validate the generalized method, three modules with different shapes were chosen. The first module is a piping system. This system was selected as the compatibility of the piping system is a challenge for construction industry. The distance between the pipes needs to pass inspection based on the construction codes. During the inspection process, the gap between two pipes is measured and based on codes and pipe diameter cannot exceed a certain threshold. The second module is a precast concrete module. The rebars in such modules are often misplaced and require reworks to be fixed. The third module is a window system. Incompatibility in window systems can cause waste of energy and rework depending on the amount of gap. Fig. 6 presents these three compatibility tasks.

Two objects per module were selected and scanned. The CAD models of these objects were also acquired. Fig. 7 shows the pictures, scanned models, and BIM models of the six objects. These objects were selected in a way that they can represent challenges (symmetricity, self-occlusion while scanning, etc.) for the compatibility checking method. The result of the experiment was generated using an Intel Core i7-6700K with 64 GB of RAM and an Nvidia GTX 1080 as the graphic card.

##### 4.1. Data collection

Faro S70 laser scanner was used to scan A1, A2, C1, and C2. The objects were placed on a table, and the data was collected using four setups around the table, as illustrated in Fig. 8. Using the FARO software called, Scene, the data from four setups were accurately registered, and the objects' point cloud was extracted. To make 3D scanned models of the small objects (B1 and B2), the authors used the Artec Leo laser scanners [47]. Artec Leo is a hand-held scanner that can achieve an accuracy of up to 0.1 mm whereas Faro S70 can reach to up to 0.3 mm. The pipe was placed on the rotary table while 3D hand-held scanner stays fixed to generate a 3D scanned model.

For each setup, the resolution was set at 1/5, meaning the scan size was chosen as (8192 by 3413 Pt). Therefore, the number of collected points in each setup was 28.0 million points. With this setting, the point-to-point distance will be 7.7 mm at a 10-m distance. Also, the quality was selected at 6×, meaning that each point was sampled six times to make sure that the point cloud is accurate and reliable. Lastly, the point clouds are cropped, and the objects' point clouds are separated from the surroundings. However, the removal of surrounding scene (or extraction of object points) can be easily automated after registration is completed [40]. Table 1 depicts the number of points in the point cloud (point count) collected from each element and the number of vertices (vertex count) for their corresponding BIM models.

##### 4.2. Data registration

To register the collected point cloud to the BIM model, six markers

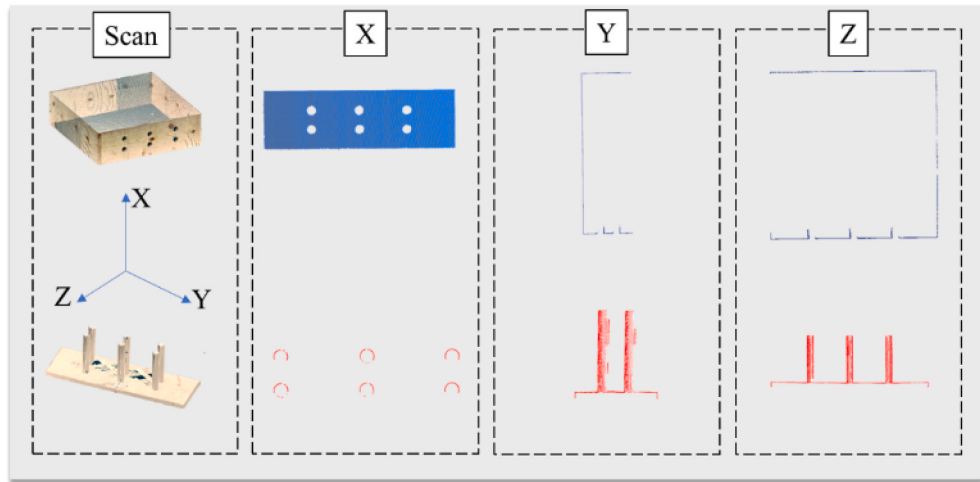


Fig. 11. Compatibility cross section for objects C1 and C2.

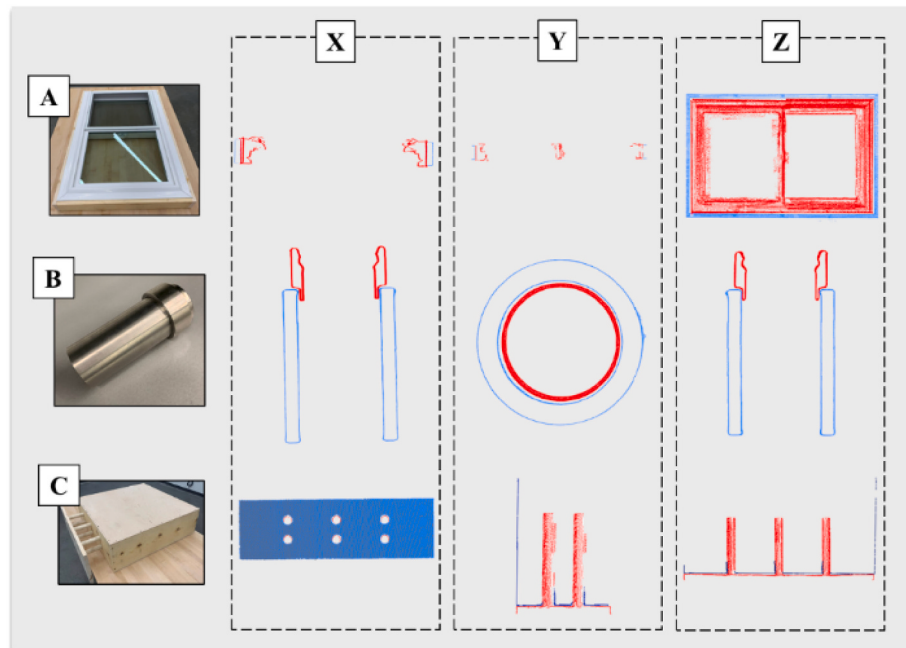


Fig. 12. Cross section of each coupling system in each direction.

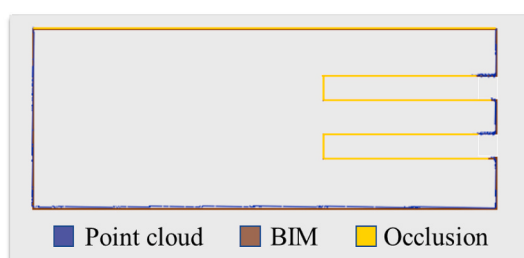


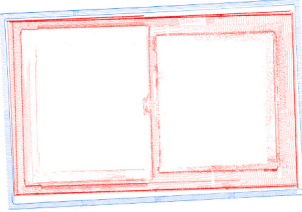
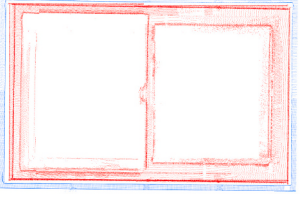
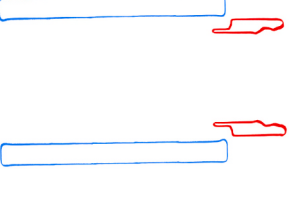
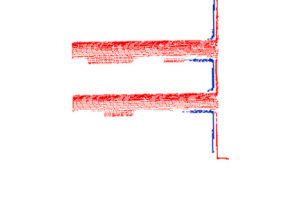
Fig. 13. 2D occlusion map for object C1 in y direction.

**Table 4**  
Compatibility feature values for each element set and time performance.

|                                    | Object set |       |       |
|------------------------------------|------------|-------|-------|
|                                    | A          | B     | C     |
| MD (mm)                            | 4          | 8     | 6     |
| MD calculation time (s)            | 0.76       | 7.39  | 0.58  |
| Cross section calculation time (s) | 0.243      | 5.12  | 0.193 |
| Total computation time (s)         | 1.003      | 12.51 | 0.773 |

were selected from both BIM and point cloud. Using these points, the BIM model and the point cloud were registered as described in [Section 3.2](#). Data registration using Cloud Compare [43]. [Table 2](#) shows the error for each marker in the six collected models in this section. The registration process was iteratively done to make sure that the registration accuracy was kept under the selected threshold for the compatibility checking. The results in [Table 2](#) show an accuracy of 1–6 mm for

**Table 5**  
Scenarios that compatibility analysis was tested on.

|                 |   | Scenarios   |   |   |     |     |     |
|-----------------|---|---|---|---|-----|-----|-----|
|                 |   | SC1   | SC2   | SC3   | SC4 | SC5 | SC6 |
| Thresholds (mm) | A1 scaled down 1 cm in x and y directions   | A1 rotated 5 degrees in z direction   | B2 rotated 5 degrees in x direction   | C2 scaled down 5 cm in y direction  |     |     |     |
| 5-10            | Incompatible  | Incompatible  | Incompatible  | Compatible  |     |     |     |
| 10-15           | Compatible  | Incompatible  | Incompatible  | Incompatible  |     |     |     |
| 15-20           | Incompatible  | Incompatible  | Incompatible  | Incompatible  |     |     |     |
| Illustration    |  |  |  |  |     |     |     |

**Table 6**  
Confidence level for each threshold based on the defined scenarios in [Table 5](#).

| Thresholds (mm) | Scenarios |     |     |     |     |     |
|-----------------|-----------|-----|-----|-----|-----|-----|
|                 | SC1       | SC2 | SC3 | SC4 | SC5 | SC6 |
| 5-10            | 16%       | 44% | 52% | 1%  | 53% | 53% |
| 10-15           | 51%       | 41% | 24% | 17% | 24% | 24% |
| 15-20           | 29%       | 7%  | 2%  | 51% | 2%  | 2%  |

registration of point clouds to the corresponding BIM elements, verifying the manufacturer claim of millimeter accuracy of point clouds.

#### 4.3. Data preprocessing

This section presents the results of noise quantification and cancellation. Unity 3D was used as the main tool for implementing the algorithms in this section and compatibility analysis section. [Table 3](#) shows the results of noise cancellation for each point clouds. Noise cancellation step ensures that the point cloud noise is minimal, and the point clouds are ready for compatibility analysis. [Fig. 9](#) shows the result of noise removal process on object C1 in [Fig. 7](#).

#### 4.4. Compatibility analysis

The last part of the method is compatibility analysis. The first step of compatibility is to generate a cross section for each module. The cross-section generation was introduced in the method section. The two main parameters in generating the point cloud cross section are the position and direction of the cross-section plane as well as the offset which is selected by the user. [Fig. 10](#) shows a sample cross section plane and offset for C1.

The [Fig. 11](#) shows the extracted cross sections of objects C1 and C2 in x, y, z direction. The offset is selected as 20 mm. The cross sections will be used to measure minimum distance between modules and generate occlusion maps that is detailed below.

Similarly for each compatibility scenario, cross sections can be generated in x, y, and z directions. [Fig. 12](#) shows cross sections of the modules in each compatibility scenarios. In each scenario, one module cross section was colored in red while the other module was in blue.

[Fig. 13](#) shows the occlusion map of the C1 in y direction. The occlusion map identifies and visualizes the parts of the model that were not scanned (i.e., due to self-occlusion or site conditions). Therefore, the system does not detect any incompatibilities in the occluded areas and the user will know the areas that are not checked. This is an inherent limitation of visual sensors that rely on clear line-of-sight (i.e., terrestrial laser scanner).

[Table 4](#) shows the results of the compatibility analysis and shows the value of each feature in each compatibility scenario (A, B, and C). The results of the compatibility analysis can be approved or rejected based on a user selected threshold. Lastly, the time performance of the compatibility analysis is reported to assess the computational complexity of the proposed algorithms. The time performance in scenario B was higher than the other two scenarios due to the large number of points in the point cloud. The reason why it had significantly more number of points (as illustrated in [Table 1](#)) in this object is that the modules in scenario B was scanned using a high precision hand-held laser scanner as opposed to the terrestrial laser scanner for the other two scenarios.

Ultimately, the objects were manipulated in six various scenarios (i.e., scaling one module in one direction or introducing twist in one module) to test its performance against different as-built deviations. The compatibility analysis was performed on all these scenarios. [Table 5](#) shows when the compatibility analysis algorithm accurately detected the incompatibilities with various thresholds and through different compatibility scenarios. In this table, different ranges have been selected (e.g., 5-10, 10-15, and 15-20). If MD was in any of the selected ranges,

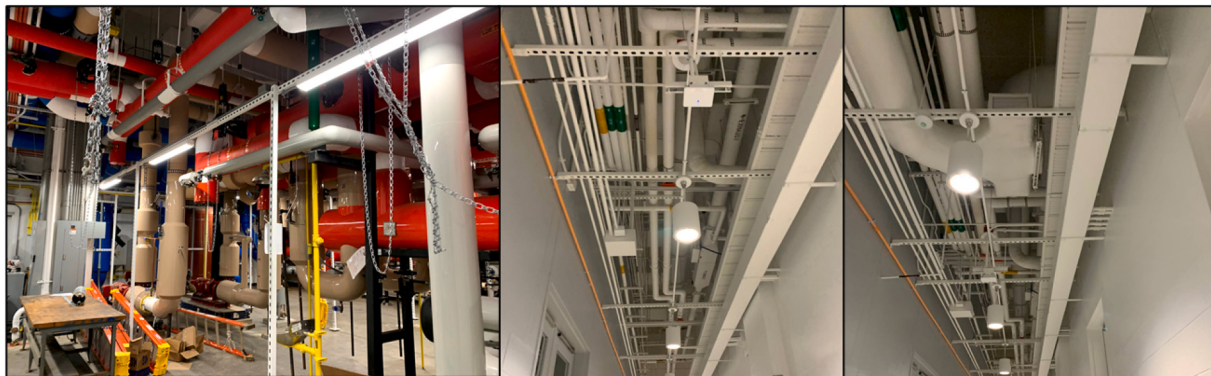


**Fig. 14.** Sample of complex mechanical systems.

the system is marked as compatible for that range. Also, [Table 5](#) summarizes the type of manipulation for each scenario (SC1 to 7), compatibility of the two parts, and a figure showing a cross section per scenario. The compatibility scenarios were manually inspected, and the compatibility decisions were accurate. To ensure that the MD is accounted for both modules error, errors from both modules has been added to the MD. Since the error in each module is a normal distribution, therefore, the summation of errors and MD will be a normal distribution which is called MD<sub>dist</sub>. Eq. (3) shows the formula to calculate MD<sub>dist</sub>.

$$\begin{aligned} MD_{dist} &= MD + N_{module\_1}(\mu_1, \sigma_1) + N_{module\_2}(\mu_2, \sigma_2) \\ &= MD + N\left(\mu_1 + \mu_2, \sqrt{\sigma_1^2 + \sigma_2^2}\right) \end{aligned} \quad (3)$$

The area under MD<sub>dist</sub> distribution will be the probability of MD being in the selected range. This probability could be used as a metric to report if the modules are compatible in each range. The assumption for compatibility analysis is that the probability (confidence level above 50% confidence level will be marked as compatible. The confidence level has been reported for each of the six scenarios in [Table 6](#). Lastly, the strength and the limitations of the compatibility analysis was discussed in the Discussion and future works section.

## 5. Discussion and future works

The proposed compatibility checking method can be used in several domains as follows. The first domain can be permitting operations. For example, in the case of concrete pipe installation, the gap between modules should not exceed a certain threshold based on local codes. The current methods for performing such operations can be done only after the modules (e.g., pipes) have been shipped and installed in place. Such procedure can often cause rework in cases where the required threshold is not met. The second domain is where the modules does not fit in place which can cause delays and rework to the project. For example, if the rebars do not fit in the holes in precast concrete modules, the compatibility analysis can easily detect that.

One of the strengths of this method is that any scanning device/technology that meets the user's quality requirement can be used. On the other hand, the main limitation of the proposed system is that the data collection process (i.e., use of terrestrial scanners) is often time consuming. In future there is a need for devices that can scan components at a much faster rate. Also, noise can adversely affect the accuracy of the proposed method. Therefore, there is a need for research efforts that can minimize the amount of noise in the point cloud especially for metallic objects (or any with reflective surfaces) as metal is one of the commonly used materials in the construction. Furthermore, the processing time of the compatibility analysis is directly correlated with the number of points in the modules. Therefore, there is a need for methods that can sample point clouds effectively and reduce the processing time especially for the point clouds that are generated with high precision

hand-held laser scanners. Lastly, the proposed compatibility checking system presented high performance on the experimented modules, however, the compatibility checking system needs.

[Fig. 14](#) shows an example of how this research fits in practice in complex construction systems and shows how the process of bringing elements virtually to the facility (could also be a construction site) and visually inspect and check for compatibility issues before shipping a prefabricated element can be beneficial. During construction, prefabricated components that arrive on a job site will not have compatibility issues after going through this process. Similarly, during operation and maintenance, any replacement parts/components (e.g., old steam generator in a power plant) that will arrive at the facility will not have any compatibility issues. Lastly, this framework can be beneficial for change orders as any changes in site condition can be scanned and compatibility with a new component/design can be assessed quickly. A user can simply proof check the new component even without having access to BIM model or drawings.

The compatibility algorithm has several limitations that need to be addressed. Firstly, having high level of noise in the scanned model point cloud could potentially fail the proposed compatibility algorithm. For example, this algorithm could not be used for point clouds that are generated using photogrammetry. Also, the objects that are transparent or metallic might introduce extensive amount of noise in the scanned model and cause the algorithm to fail. Moreover, several steps involve manual processes, such as registration, selection of cross-section plane, and offset for compatibility. These manual steps could be automated by integrating automated registration methods similar to [15,44] and methods to select the compatibility plane and offset using learning-based method that imitate human agent.

## 6. Conclusion

Over the past few years, reality capture technologies have received significant popularity in the AEC industry, namely construction progress monitoring [21], assembly training [15], construction quantity takeoff [24], safety [25,48], and inspection [23]. However, there are still numerous research questions to be investigated, such as efficient and general compatibility checking of offsite components. To address this issue and improve the compatibility checking process, this paper presents a generalized method for compatibility checking of fabricated components. The proposed method is a powerful tool in detecting geometric defects and incompatibilities between modules in modular construction. This compatibility system is robust to occlusions, noise, and can be applied on various types of point clouds that are captured using different approaches and devices. The system was tested and validated in three different scenarios and demonstrated the effectiveness and robustness of the proposed method for compatibility analysis on the as-built elements and verified the compatibility of the as-built models.

## Declaration of Competing Interest

None.

## Data availability

The data that has been used is confidential.

## Acknowledgments

This work was partially funded under the Versatile Test Reactor Program of the US Department of Energy (DOE) by Battelle Energy Alliance, LLC (BEA), the Management and Operating Contractor of Idaho National Laboratory (INL) under Contract Number DE-AC07-05ID14517 with DOE and DOE's ARPE-E Program under Award Number DE-AR0001155. The United States Government has a non-exclusive, paid-up, irrevocable, worldwide license to publish and reproduce the published form of this work and allow others to do so, for United States Government purposes. Any opinions, findings, conclusions and/or recommendations expressed in this paper are those of the authors and do not reflect the views of the entities above.

## References

- [1] United States Census Bureau, Construction Spending. <https://www.census.gov/construction/c30/pdf/release.pdf>, 2020. Accessed date: January 20, 2020.
- [2] M. Noghabaei, A. Heydarian, V. Balali, K. Han, Trend analysis on adoption of virtual and augmented reality in the architecture, engineering, and construction industry, Data. 5 (2020), <https://doi.org/10.3390/data5010026>.
- [3] H. Karimi, T.R.B. Taylor, G.B. Dadi, P.M. Goodrum, C. Srinivasan, Impact of skilled labor availability on construction project cost performance, J. Constr. Eng. Manag. 144 (2018) 04018057, [https://doi.org/10.1061/\(ASCE\)CO.1943-7862.0001512](https://doi.org/10.1061/(ASCE)CO.1943-7862.0001512).
- [4] S. Kim, S. Chang, D. Castro-Lacouture, Dynamic modeling for analyzing impacts of skilled labor shortage on construction project management, J. Manag. Eng. 36 (2020) 04019035, [https://doi.org/10.1061/\(ASCE\)ME.1943-5479.0000720](https://doi.org/10.1061/(ASCE)ME.1943-5479.0000720).
- [5] H. Li, C. Zhang, S. Song, S. Demirkesen, R. Chang, Improving tolerance control on modular construction project with 3d laser scanning and bim: a case study of removable floodwall project, Appl. Sci. 10 (2020) 1–21, <https://doi.org/10.3390/app10238680>.
- [6] Y. Yang, M. Pan, W. Pan, 'Co-evolution through interaction' of innovative building technologies: the case of modular integrated construction and robotics, Autom. Constr. 107 (2019), 102932, <https://doi.org/10.1016/j.autcon.2019.102932>.
- [7] W. Lu, H. Yuan, Investigating waste reduction potential in the upstream processes of offshore prefabrication construction, Renew. Sust. Energ. Rev. 28 (2013) 804–811, <https://doi.org/10.1016/J.RSER.2013.08.048>.
- [8] Z. Li, G.Q. Shen, M. Alshawi, Measuring the impact of prefabrication on construction waste reduction: an empirical study in China, Resour. Conserv. Recycl. 91 (2014) 27–39, <https://doi.org/10.1016/J.RESCONREC.2014.07.013>.
- [9] Y. Shahtaheri, C. Rausch, J. West, C. Haas, M. Nahangi, Managing risk in modular construction using dimensional and geometric tolerance strategies, Autom. Constr. 83 (2017) 303–315, <https://doi.org/10.1016/j.autcon.2017.03.011>.
- [10] H. Hyun, H. Kim, H.S. Lee, M. Park, J. Lee, Integrated design process for modular construction projects to reduce rework, Sustainability. 12 (2020) 530, <https://doi.org/10.3390/su12020530>.
- [11] J. Guo, Q. Wang, J.H. Park, Geometric quality inspection of prefabricated MEP modules with 3D laser scanning, Autom. Constr. 111 (2020), 103053, <https://doi.org/10.1016/j.autcon.2019.103053>.
- [12] M. Safa, A. Shahi, M. Nahangi, C. Haas, H. Noori, Automating measurement process to improve quality management for piping fabrication, Structures. 3 (2015) 71–80, <https://doi.org/10.1016/j.istruc.2015.03.003>.
- [13] Q. Wang, M.K. Kim, J.C.P. Cheng, H. Sohn, Automated quality assessment of precast concrete elements with geometry irregularities using terrestrial laser scanning, Autom. Constr. 68 (2016) 170–182, <https://doi.org/10.1016/j.autcon.2016.03.014>.
- [14] M.K. Kim, J.P.P. Thedja, Q. Wang, Automated dimensional quality assessment for formwork and rebar of reinforced concrete components using 3D point cloud data, Autom. Constr. 112 (2020), 103077, <https://doi.org/10.1016/j.autcon.2020.103077>.
- [15] M. Noghabaei, K. Han, Object manipulation in immersive virtual environments: hand motion tracking technology and snap-to-fit function, Autom. Constr. 124 (2021), <https://doi.org/10.1016/j.autcon.2021.103594>.
- [16] X. Zhou, J. Liu, G. Cheng, D. Li, Y.F. Chen, Automated locating of replaceable coupling steel beam using terrestrial laser scanning, Autom. Constr. 122 (2021), 103468, <https://doi.org/10.1016/j.autcon.2020.103468>.
- [17] M. Noghabaei, K. Asadi, K. Han, Virtual manipulation in an immersive virtual environment: simulation of virtual assembly, computing in civil engineering: visualization, Inform. Model. Simul. (2019) 95–102, <https://doi.org/10.1061/9780784482421.013>.
- [18] D. Li, J. Liu, L. Feng, Y. Zhou, H. Qi, Y.F. Chen, Automatic modeling of prefabricated components with laser-scanned data for virtual trial assembly, Comput. Aid. Civ. Infrastruct. Eng. (2020), <https://doi.org/10.1111/mice.12627>.
- [19] Q. Wang, J.C.P. Cheng, H. Sohn, Automated estimation of reinforced precast concrete rebar positions using colored laser scan data, computer-aided civil and infrastructure, Engineering. 32 (2017) 787–802, <https://doi.org/10.1111/mice.12293>.
- [20] Y. Tan, S. Li, Q. Wang, Automated geometric quality inspection of prefabricated housing units using BIM and LiDAR, Remote Sens. 12 (2020) 2492, <https://doi.org/10.3390/RS12152492>.
- [21] K. Asadi, H. Ramshankar, M. Noghabaei, K. Han, Real-time image localization and registration with BIM using perspective alignment for indoor monitoring of construction, J. Comput. Civ. Eng. (2019), [https://doi.org/10.1061/\(ASCE\)CP.1943-5487.0000847](https://doi.org/10.1061/(ASCE)CP.1943-5487.0000847).
- [22] M. Golparvar-Fard, J. Bohn, J. Teizer, S. Savarese, F. Peña-Mora, Evaluation of image-based modeling and laser scanning accuracy for emerging automated performance monitoring techniques, Autom. Constr. 20 (2011) 1143–1155, <https://doi.org/10.1016/J.AUTCON.2011.04.016>.
- [23] C.H.P. Nguyen, Y. Choi, Comparison of point cloud data and 3D CAD data for on-site dimensional inspection of industrial plant piping systems, Autom. Constr. 91 (2018) 44–52, <https://doi.org/10.1016/j.autcon.2018.03.008>.
- [24] M. Kamari, Y. Ham, Vision-based volumetric measurements via deep learning-based point cloud segmentation for material management in jobsites, Autom. Constr. 121 (2021), 103430, <https://doi.org/10.1016/j.autcon.2020.103430>.
- [25] I. Jeelani, K. Asadi, H. Ramshankar, K. Han, A. Albert, Real-time vision-based worker localization & hazard detection for construction, Autom. Constr. 121 (2021), 103448, <https://doi.org/10.1016/j.autcon.2020.103448>.
- [26] M. Farhadmanesh, C. Cross, A.H. Mashhadi, A. Rashidi, J. Wempen, Highway asset and pavement condition management using mobile photogrammetry, Transp. Res. Rec. (2021), <https://doi.org/10.1177/03611981211001855>.
- [27] M. Nahangi, J. Yeung, C.T. Haas, S. Walbridge, J. West, Automated assembly discrepancy feedback using 3D imaging and forward kinematics, Autom. Constr. 56 (2015) 36–46, <https://doi.org/10.1016/j.autcon.2015.04.005>.
- [28] M. Nahangi, C.T. Haas, Automated 3D compliance checking in pipe spool fabrication, Adv. Eng. Inform. 28 (2014) 360–369, <https://doi.org/10.1016/j.aei.2014.04.001>.
- [29] T. Czerniawski, M. Nahangi, C. Haas, S. Walbridge, Pipe spool recognition in cluttered point clouds using a curvature-based shape descriptor, Autom. Constr. 71 (2016) 346–358, <https://doi.org/10.1016/j.autcon.2016.08.011>.
- [30] Z. Wang, Q. Zhang, B. Yang, T. Wu, K. Lei, B. Zhang, T. Fang, Vision-based framework for automatic progress monitoring of precast walls by using surveillance videos during the construction phase, J. Comput. Civ. Eng. 35 (2021) 04020056, [https://doi.org/10.1061/\(asce\)cp.1943-5487.0000933](https://doi.org/10.1061/(asce)cp.1943-5487.0000933).
- [31] M. Nahangi, C.T. Haas, Skeleton-based discrepancy feedback for automated realignment of industrial assemblies, Autom. Constr. 61 (2016) 147–161, <https://doi.org/10.1016/J.AUTCON.2015.10.014>.
- [32] M.K. Kim, H. Sohn, C.C. Chang, Automated dimensional quality assessment of precast concrete panels using terrestrial laser scanning, Autom. Constr. 45 (2014) 163–177, <https://doi.org/10.1016/j.autcon.2014.05.015>.
- [33] M.K. Kim, J.C.P. Cheng, H. Sohn, C.C. Chang, A framework for dimensional and surface quality assessment of precast concrete elements using BIM and 3D laser scanning, Autom. Constr. 49 (2015) 225–238, <https://doi.org/10.1016/j.autcon.2014.07.010>.
- [34] H. Alzraiee, R. Sprotte, A. Leal Ruiz, Quality control for concrete steel embed plates using LiDAR and point cloud mapping, in: Proceedings of the 37th International Symposium on Automation and Robotics in Construction (ISARC), 2020, <https://doi.org/10.22260/ISARC2020/0101>.
- [35] M.S.A. Enshassi, S. Walbridge, J.S. West, C.T. Haas, Dynamic and proactive risk-based methodology for managing excessive geometric variability issues in modular construction projects using Bayesian theory, J. Constr. Eng. Manag. 146 (2020) 04019096, [https://doi.org/10.1061/\(asce\)co.1943-7862.0001747](https://doi.org/10.1061/(asce)co.1943-7862.0001747).
- [36] G. Cha, S. Park, T. Oh, A terrestrial LiDAR-based detection of shape deformation for maintenance of bridge structures, J. Constr. Eng. Manag. 145 (2019) 04019075, [https://doi.org/10.1061/\(asce\)co.1943-7862.0001701](https://doi.org/10.1061/(asce)co.1943-7862.0001701).
- [37] E.B. Anil, P. Tang, B. Akinci, D. Huber, Deviation analysis method for the assessment of the quality of the as-is building information models generated from point cloud data, Autom. Constr. 35 (2013) 507–516, <https://doi.org/10.1016/J.AUTCON.2013.06.003>.
- [38] M. Rumpler, S. Daftry, A. Tscharf, R. Pretenthaler, C. Hoppe, G. Mayer, H. Bischof, Automated End-to-End Workflow for Precise and Geo-Accurate Reconstructions using Fiducial Markers, 2014, <https://doi.org/10.5194/isprsaannals-II-3-135-2014>.
- [39] K.K. Han, M. Golparvar-Fard, Appearance-based material classification for monitoring of operation-level construction progress using 4D BIM and site photologs, Autom. Constr. 53 (2015) 44–57, <https://doi.org/10.1016/J.AUTCON.2015.02.007>.
- [40] K. Han, J. Degol, M. Golparvar-Fard, Geometry- and appearance-based reasoning of construction progress monitoring, J. Constr. Eng. Manag. 144 (2018) 04017110, [https://doi.org/10.1061/\(ASCE\)CO.1943-7862.0001428](https://doi.org/10.1061/(ASCE)CO.1943-7862.0001428).
- [41] B.K.P. Horn, Closed-form solution of absolute orientation using unit quaternions, J. Opt. Soc. Am. A 4 (1987) 629–642, <https://doi.org/10.1364/JOSAA.4.000629>.
- [42] D. Aiger, N.J. Mitra, D. Cohen-Or, 4-points congruent sets for robust pairwise surface registration, in: SIGGRAPH'08: International Conference on Computer Graphics and Interactive Techniques, ACM SIGGRAPH 2008 Papers 2008 27, 2008, p. 1, <https://doi.org/10.1145/1399504.1360684>.

- [43] D. Girardeau-Montaut, Cloud Compare Open Source Project. <https://www.cloudcompare.org/main.html>, 2011. Accessed date: May 29, 2022.
- [44] C. Kim, M. Kim, J. Martínez-Sánchez, N.A. Sheik, G. Deruyter, P. Veelaert, Plane-based robust registration of a building scan with its BIM, *Remote Sens.* 14 (2022) 1979, <https://doi.org/10.3390/RS14091979>.
- [45] C. Compare, SOR Filter - CloudCompareWiki. [https://www.cloudcompare.org/doc/wiki/index.php?title=SOR\\_filter](https://www.cloudcompare.org/doc/wiki/index.php?title=SOR_filter), 2021.
- [46] H. Balta, J. Velagic, W. Bosschaerts, G. De Cubber, B. Siciliano, Fast statistical outlier removal based method for large 3D point clouds of outdoor environments, IFAC-PapersOnLine. 51 (2018) 348–353, <https://doi.org/10.1016/j.ifacol.2018.11.566>.
- [47] Artec Leo 3D Scanner - The first scanner to offer automatic onboard processing. <https://sourcegraphics.com/3d/scanners/artec/leo/>, 2020. Accessed date: March 2, 2020.
- [48] M. Noghhabaei, K. Han, A. Albert, Feasibility study to identify brain activity and eye-tracking features for assessing Hazard recognition using consumer-grade wearables in an immersive virtual environment, *J. Constr. Eng. Manag.* 147 (2021) 04021104, [https://doi.org/10.1061/\(ASCE\)CO.1943-7862.0002130](https://doi.org/10.1061/(ASCE)CO.1943-7862.0002130).